Nonlinear dynamics in PEH for enhanced power output and vibration suppression in metastructures

Alimohammadi, Hossein; Vassiljeva, Kristina; HosseinNia, S. Hassan; Petlenkov, Eduard

DOI
10.1007/s11071-024-09739-w

Publication date
2024

Document Version
Final published version

Published in
Nonlinear Dynamics

Citation (APA)
Alimohammadi, H., Vassiljeva, K., HosseinNia, S. H., & Petlenkov, E. (2024). Nonlinear dynamics in PEH for enhanced power output and vibration suppression in metastructures. *Nonlinear Dynamics*, *112*(15), 12941-12963. https://doi.org/10.1007/s11071-024-09739-w

Nonlinear Dyn
https://doi.org/10.1007/s11071-024-09739-w

ORIGINAL PAPER

Nonlinear dynamics in PEH for enhanced power output and vibration suppression in metastructures

Hossein Alimohammadi · **Kristina Vassiljeva** · **S. Hassan HosseinNia** · **Eduard Petlenkov**

Received: 2 November 2023 / Accepted: 8 May 2024

Abstract This study delves into the nonlinear dynamics of metamaterials, exploring the dual objective of enhancing power output and achieving vibration suppression through piezoelectric energy harvesters (PEHs). Our approach is structured into a sequence of increasingly complex models that bridge mechanical resonators with their electromechanical counterparts. We initiate with (1) modeling mechanical resonators, incorporating nonlinear behaviors that are often overlooked in the linear domain. This lays the groundwork for understanding the fundamental mechanisms of vibration within metamaterials. Subsequently, we progress to (2) electromechanical resonators, where piezoelectric components are integrated, revealing a richer dynamic landscape that is influenced by the interplay of mechanical and electrical energies. The latter sections of our investigation introduce and examine (3) mechanical and (4) electromechanical internally coupled resonators. These segments unveil the role of internal couplings in steering the metamaterial's energy harvesting capabilities and its resilience to vibrational disturbances. Through meticulous simulations and analysis, the research brings to light the significant influence of specific PEH nonlinear parameters on the system's efficiency, offering insights for the optimization of PEHs in practical applications.

Keywords Nonlinear dynamics · Piezoelectric energy harvesting · Electromechanical nonlinearity · Internally coupled resonators · Vibration suppression · Lumped parameter model

H. Alimohammadi (✉) · K. Vassiljeva · E. Petlenkov
Department of Computer Systems, Tallinn University of Technology, 2618 Tallinn, Estonia
e-mail: hossein.alimohammadi@taltech.ee

K. Vassiljeva
e-mail: kristina.vassiljeva@taltech.ee

S. H. HosseinNia
Department of Precision and Microsystems Engineering, Delft University of Technology, 2628CD Delft, The Netherlands
e-mail: s.h.hosseinniakani@tudelft.nl

E. Petlenkov
Department of Computer Systems, Akadeemia tee 15a, 12618 Tallinn, Estonia
e-mail: eduard.petlenkov@taltech.ee

1 Introduction

The advent of mechanical metamaterials, characterized by their unique ability to control vibrational energy, has revolutionized the design and application of energy harvesting systems. For instance, the work by Jiao et al. highlights how modern mechanical metamaterials can interact with their environment and adapt to various conditions, offering insights into the design and optimization of these innovative materials [1]. Central to this innovation are the piezoelectric energy harvesters (PEHs) that form a chain of oscillators, each capable of converting vibrational energy into electrical power. This paper focuses on the detailed study and enhance-

Published online: 29 May 2024

ment of such systems through the lens of nonlinear dynamics, [2,3].

Our investigation begins by defining the mechanical and electromechanical metamaterial system that forms the basis of our theoretical models. We consider a chain of mechanical oscillators, each linked to a piezoelectric resonator, forming an electromechanical system that spans both the mechanical and electrical domains. This interconnected system not only offers the promise of energy harvesting but also presents a platform for vibration suppression-two objectives that are often at odds in traditional materials.

The objective of this study is twofold: to explore the underlying nonlinear dynamic behavior of the metamaterial/electromechanical system and to optimize the design for maximum power output while minimizing vibrational disturbances. To this end, we develop comprehensive theoretical models that capture the intricate behaviors of the resonators and their electromechanical interactions. These models are rigorously validated through a series of numerical simulations that not only ensure the theoretical models align with expected outcomes but also establish comprehensive metrics for evaluating the performance of the energy harvesters.

In summary, this research sets the stage for an in-depth exploration of PEHs within the realm of metamaterials. By addressing the nonlinear dynamics inherent to these systems, we aim to unveil strategies for enhanced energy harvesting and vibration mitigation. The key contributions of this paper are summarized as follows:

- Development of comprehensive theoretical models that integrate both mechanical and electromechanical aspects of piezoelectric energy harvesters within mechanical metamaterials, offering new insights into their nonlinear dynamic behavior.
- A detailed analysis of the impact of various forms of nonlinearity on the performance of energy harvesters, including mechanical and electromechanical nonlinearities, thereby extending the understanding of their operation and optimization.
- Introduction of novel metrics for evaluating the effectiveness of energy harvesters, bridging the gap between theoretical analysis and practical application, and paving the way for future research in optimizing metamaterial-based energy harvesting systems.
- Validation of the theoretical models through rigorous numerical simulations, ensuring their accuracy and reliability, and providing a solid foundation for future experimental investigations.

The structure of the remaining sections of this paper is organized as follows: Sect. 2 delves into the background and relevant literature, laying the groundwork for understanding the current state of research in piezoelectric energy harvesting. Section 3 outlines the methodology employed in this study, including mathematical modeling and simulation approaches. Section 4 presents the results and discussions, where the findings from the application of the proposed models are analyzed and interpreted. Section 5 details the contributions and findings related to nonlinear electromechanical dynamics and their impact on piezoelectric energy harvesters. Section 6 introduces internally coupled resonators with a focus on electromechanical nonlinearity, exploring their implications for energy harvesting. Finally, Sect. 7 concludes the paper with a summary of the findings, contributions to the field, and suggestions for future research directions.

2 Background

The field of energy harvesting has seen significant advancements with the integration of piezoelectric materials into mechanical metamaterials. These materials, capable of converting mechanical vibrations into electrical energy, have opened new avenues for creating efficient energy harvesters. Central to the design of these systems are chain oscillators, which play a dual role in energy conversion and vibration suppression [4,5]. Chain oscillators are fundamental in mechanical metamaterials, designed to control vibrational energy flow through the system while maximizing energy extraction from ambient sources [6].

2.1 The role of nonlinearities in energy harvesting

Nonlinear dynamics play a pivotal role in enhancing the performance of energy harvesting systems [7]. Both mechanical and electromechanical nonlinearities introduce complex behaviors such as bifurcations and chaos, extending the frequency range over which energy can be efficiently harvested. Recent advancements have led

to a deeper understanding and exploitation of nonlinearities within PEHs. Through resonators, the vibration suppression and energy harvesting capabilities of nonlinear models for PEHs have been thoroughly analyzed. These models highlight the role of nonlinear dynamics in enhancing PEH performance, offering insights for more efficient energy solutions. Daqaq et al. [8] found that nonlinear vibratory energy harvesters are more adaptable and efficient in varied environments than their linear counterparts, due to their broader frequency response. This makes them a potentially superior option for powering low-power devices. Furthermore, recent research by Daqaq [9] has extended the nonlinear dynamics to practical applications, specifically focusing on how weakly nonlinear energy harvesters can effectively charge batteries under various excitations, offering a balance between simplicity and accuracy in their analytical models.

2.2 Chain oscillators in mechanical metamaterials

Chain oscillators form the backbone of mechanical metamaterials used in energy harvesting applications. Their primary function is to suppress undesirable vibrations while facilitating the transfer of mechanical energy to piezoelectric elements for conversion into electrical energy. The integration of chain oscillators with piezoelectric resonators exemplifies the synergy between mechanical and electrical components in metamaterials [10]. By designing the oscillators to exploit specific nonlinear dynamics, it is possible to achieve optimal conditions for energy harvesting, wherein the system's natural frequency aligns with prevalent ambient vibrations. Furthermore, the suppression of vibrations through chain oscillators enhances the lifespan and reliability of the harvesting system [11].

In the quest for optimized energy harvesting systems, the exploration of nonlinear dynamics within mechanical and electromechanical systems has emerged as a critical area of research. These nonlinearities, whether inherent in the mechanical structure or introduced through electromechanical coupling, significantly influence the system's ability to harvest energy and suppress vibrations [12]. As such, understanding and leveraging these nonlinear effects can lead to substantial improvements in PEH performance. This backdrop of nonlinear dynamics sets the stage for an in-depth examination of mechanical and electromechanical nonlinearities in PEHs. The following sections delve into the mechanical nonlinearity of resonators, the electromechanical nonlinearity of resonators, and the nuanced dynamics of internally coupled resonators with both mechanical and electromechanical nonlinearities. Each area offers unique insights into the potential for advancing energy harvesting technologies, underscoring the complex interplay between mechanical structures and piezoelectric elements in metamaterials designed for optimized energy conversion

2.3 Nonlinearity in energy harvesters and metamaterial chains

The exploration of mechanical nonlinearities in energy harvesters and metamaterial chains reveals their significant impact on enhancing energy conversion efficiency and vibration control capabilities. This line of inquiry delves into how the introduction of nonlinear properties to resonators, specifically those exhibiting mildly cubic nonlinearities, influences the behavior of acoustic metamaterials and, consequently, the performance of energy harvesting systems (see Fig. 1).

Local resonators within periodic chains, when embedded with nonlinearities, are shown to initiate a detailed wave response, providing an intricate interaction within the system. This interaction is pivotal, as it shapes the system's capability to adapt and respond to vibrational energies more effectively [13,14]. The dynamics of wave propagation in these metamaterials are fundamentally altered by the integration of resonators embedded with mildly cubic nonlinearities, leading to modifications in the frequency domain where energy harvesting and vibration suppression are optimized [15,16]. The study of systems where periodic chains integrate multiple local resonators, each exhibiting nonlinear behavior, has highlighted the potential for expanding the operational bandwidth of energy harvesters. Such systems are adept at adapting to a wider range of vibrational frequencies, thereby enhancing the efficiency of energy conversion. Additionally, the incorporation of bistable systems within these metamaterial chains introduces a dynamic range of wave control, extending the capabilities of these systems beyond conventional linear models [17,18]. The chaotic behavior induced by high-intensity excitations in bistable systems allows for a broader attenuation of vibra-

tions, showcasing the advanced potential of nonlinear mechanical metamaterials in energy harvesting and vibration suppression [19]. However, experimental studies such as those by Khasawneh and Daqaq in [20], have challenged theoretical predictions about bistability in energy harvesters, showing that while bistable systems can shift operational bandwidths to lower frequencies, they may not always enhance the effective bandwidth compared to linear systems.

Bridging the concepts from nonlinear mechanical behaviors to electromechanical nonlinearities, it becomes evident that the complexity of energy harvesters is magnified when electrical components are introduced. This transition from purely mechanical to electromechanical systems opens up a broader spectrum for energy conversion efficiency and dynamic response control, setting the stage for a deeper exploration into the multifaceted nature of piezoelectric energy harvesters.

The exploration of electromechanical nonlinearity in piezoelectric energy harvesters is fundamental for advancing the efficiency and functionality of these systems. The nonlinear interactions between mechanical vibrations and electrical responses in PEHs, often mediated by components such as diodes and piezoelectric materials, play a crucial role in energy conversion dynamics.

Diodes introduce a marked non-linearity in the current–voltage relationship, significantly impacting energy harvesting efficiency. This effect is critical in rectifying the alternating current (AC) generated by piezoelectric elements into direct current (DC), which is more readily used by electronic devices [21–23]. Moreover, the interaction between mechanical structures and embedded piezoelectric materials leads to nonlinear behaviors such as amplitude-dependent frequency shifts, essential for enhancing the energy harvester's bandwidth [24,25].

The integration of data-driven methods, particularly neural networks, into PEH systems, has significantly advanced their performance, [26,27]. By leveraging smart electronic chips programmed based on these models, these systems can dynamically adapt to varying operational conditions, optimizing energy conversion efficiency in real-time. These chips, designed to handle nonlinear dynamics, enhance the adaptability and efficiency of PEHs, ensuring maximum energy extraction from environmental vibrations. This innovative approach, which combines the precision of empirical data analysis with cutting-edge electronic technology, marks a significant step forward in making energy harvesting systems more effective, reliable, and versatile.

2.4 Standard piezoelectric circuit for energy harvesting

The primary goal when integrating metamaterials into energy harvesting systems is to minimize vibrations within the main chain of the device. This minimization leads to the dissipation of the base or excitation energy primarily through the resonators attached to the system. In essence, reducing vibration in the main chain results in increased vibration within the resonators [28]. By effectively transferring energy from the main chain to the resonators, metamaterials not only protect the structural integrity of the system but also enhance the resonator's energy harvesting capabilities. This strategic distribution of vibrational energy is foundational to maximizing the efficiency of energy capture from ambient vibrations, marking a significant advancement in the development of sustainable energy solutions [29].

While metamaterials with resonators can enhance the energy capture capability, the rectifier circuit plays a pivotal role in processing this harvested energy, making it suitable for practical applications. Traditional energy harvesting circuits, characterized by their simplicity, directly connect the load to the harvesting component but often fall short in energy conversion efficiency.

Advanced circuit designs such as Synchronized Switch Harvesting on Inductor (SSHI), Synchronous Electric Charge Extraction (SECE), and Maximum Power Point Tracking (MPPT) [30–32] have been developed to address these limitations, substantially improving energy conversion efficiency. These systems not only surpass traditional models in efficiency but also adapt dynamically to varying environmental conditions to extract optimal energy. Recent progress in this field has been comprehensively reviewed in studies such as the work by Wang et al. [33] highlighting the evolution of interface circuits that significantly contribute to the efficiency and adaptability of PEHs.

Transitioning from the exploration of energy harvesting circuits to the study of internally coupled mechanical resonators, this shift underscores the integration of advanced energy conversion techniques with strategic vibration management. Through this, the

emphasis on mechanical nonlinearity within resonators emerges as a critical factor in enhancing both energy capture efficiency and system stability, signifying a comprehensive approach to optimizing metamaterial-based energy harvesting systems. Introducing nonlinearity into periodic chains with local resonators triggers wave responses that are shaped by the interplay of nonlinearity and local resonance effects. Studies on linear chains with nonlinear resonators [13,15,34] and nonlinear chains with linear resonators [15,35] have demonstrated this phenomenon.

Internally coupled mechanical resonators have emerged recently in modern dynamics and vibration control research. By harnessing the intricate interactions between internal structural elements, these resonators display a diverse range of vibrational behaviors. These characteristics offer unprecedented capabilities in manipulating and controlling wave propagation, making them invaluable assets in areas like structural health monitoring, acoustic metamaterials, and vibration mitigation. One of the pioneering research in this domain, as exemplified by studies like that of Hu et al. [36], has explored metastructures integrated with linearly coupled resonators. Their investigations reveal the presence of an additional narrow bandgap compared to conventional metastructures, highlighting the intriguing prospects of this research area.

Building upon this foundation, recent advancements have seen the development of metastructures incorporating coupled mechanical resonators with inherent nonlinearities. Notably, work by Alimohammadi et al. [37] delves into metastructures that employ a distributed parameter model for the main structure while utilizing a chain or lumped model for resonators. This approach introduces nonlinear internally coupled resonators, demonstrating enhanced wave manipulation capabilities. Their findings, showcasing the frequency response of such systems can affect the performance of metastructures with nonlinear internally coupled resonators compared to their linear counterparts. Nevertheless, a significant research gap persists in the area of nonlinear internally coupled resonators.

Transitioning from mechanical nonlinearity in internal coupled resonators, the focus shifts to electromechanical systems, where piezoelectric elements reveal intricate interactions between mechanical and electrical energies. This area, rich with potential for advancing energy harvesting and vibration control, remains largely unexplored, pointing to significant opportunities for research. In electromechanical resonators, the concept of internally coupled configurations, particularly when piezoelectric elements are interconnected, introduces a captivating complexity. These arrangements initiate a profound interaction between the mechanical and electrical domains, leading to unexpected wave propagation characteristics. Yet, despite the potential they harbor, exploration into nonlinear, internally coupled electromechanical systems remains notably limited.

This gap in the research landscape underscores the need for a comprehensive understanding of such systems, which promises to redefine the boundaries of vibration control and energy harvesting. By leveraging electromechanical nonlinearities, this design strategy enhances the efficiency and adaptability of energy harvesting systems. Studies such as those by Hu et al. and Silva et al. [25,36] underline the potential of this methodology in broadening the bandwidth for vibration suppression and energy harvesting. The integration of piezoelectric shunt techniques not only facilitates the adjustment of system dynamics but also aids in the creation of tunable band gaps.

3 Methodology

The lumped parameters model approach simplifies the analysis of a complex physical system by assuming that the system's physical properties, such as inertia, elasticity, and damping are concentrated at specific points or elements. Each element is characterized by a set of parameters, such as resistance, capacitance, and inductance for electrical circuits, or mass, damping, and stiffness for mechanical systems. These elements are interconnected in a network described by ordinary differential equations. Lumped parameter models are commonly employed when the wavelength of wave propagation is significantly larger than the dimensions of the structure, enabling the use of simplified assumptions.

3.1 Nonlinear mechanical resonators

The simplest lumped model of a 1D nonlinear phononic medium repeating unit cell, as illustrated in Fig. 1, is characterized as a linear atomic chain with embedded nonlinear resonators. This chain comprises an infinite series of uniform unit cells. Each of these unit cells

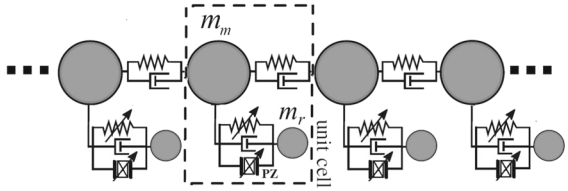

Fig. 1 Foundational models of nonlinear phononic media: a linear monoatomic chain with nonlinear resonators of masses, spring, damping, and piezoelectric element, PZ. Dashed rectangle is unit cell

consists of a mass, m_m, pertaining to the monoatomic chain, interconnected through linear springs. This primary linear chain is interfaced with nonlinear resonators, each identified by its mass, m_r. Both the damping element and the piezoelectric force of the resonators are neglected for simplicity. The net force exerted by the nonlinear spring connecting the resonators can be represented as:

$$f_r = k_r\delta + \sum \gamma_q \delta^q, \tag{1}$$

where δ is the relative displacement between the adjacent masses (chain mass and resonator). Subsequently, the dynamics of the system can be expounded as follows:

$$\begin{aligned} &m_m\ddot{u}_m + k_m\,(2u_m - u_{m^-} - u_{m^+}) \\ &\quad + \sum \gamma_{q_m}\left((u_m - u_{m^-})^q + (u_m - u_{m^+})^q\right) \\ &\quad + k_r(u_m - u_r) + \sum \gamma_{q_r}\,(u_m - u_r)^q = 0 \end{aligned} \tag{2}$$

$$m_r\ddot{u}_r - k_r\,(u_m - u_r) - \sum \gamma_{q_r}\,(u_m - u_r)^q = 0, \tag{3}$$

where for the last mass in the chain: $u_m - u_{m^+} = 0$, $\dot{u}_m - \dot{u}_{m^+} = 0$, and for the first mass in the chain: $u_{m^-} = u_b$. Here, $\gamma_{q_m}, \gamma_{q_r}$ denote the nonlinear stiffness of the monoatomic chain and resonator, respectively. Here, u_m denotes the displacement of the m^{th} mass, k_m represents the stiffness of that mass, k_r is the resonator's stiffness, while u_{m^+} and u_{m^-} indicate the displacements of the succeeding and preceding masses, respectively, and u_b signifies the displacement of the excitation at the base or first mass chain.

The parameter q can assume values $(0, 1, 2, 3, \ldots)$, denoting the degree of system nonlinearity: linear ($q = 0, 1$), quadratic ($q = 2$), cubic ($q = 3$), and so forth. Weakly and strongly nonlinear systems can be distinguished based on the relative magnitude of the nonlinear force term, expressed as $\sum \gamma_q \delta^q$. Essentially nonlinear systems are characterized by vanishing linear forces ($k_{m,r} \to 0$) but non-zero nonlinear forces ($\gamma > 0$ for all q except $q = 0$ and $q = 1$).

Cubic nonlinearities can manifest as either purely hardening ($\gamma > 0$) or softening ($\gamma < 0$), while quadratic nonlinearities combine both softening and hardening behaviors. The versatility of this elementary discrete model extends to representing more intricate media configurations. These adaptations empower discrete modeling techniques to provide insights into the complexities of nonlinear phenomena.

Considering wave propagation in a system and applying boundary conditions with an input $u_b = e^{i\omega t}$, the transmittance of the system can be quantified as $\tau = \left|\frac{u_m^N}{u_m^1}\right|$, where u_m^{N} represents the displacement of u_m at the end of the chain sequence, while u_m^1 denotes the displacement of the mass at the first position in the sequence or the base excitation or the displacement at the initial position u_b.

The Laplace transform of nonlinear terms, specifically $\gamma_{q_r}\,(u_m - u_r)^q$, is not straightforward. While one could approach this by linearizing around a specific operating point, a more practical solution is often to address it numerically. Essentially, due to the complexities introduced by nonlinearity, numerical methods frequently provide the most feasible approach for analysis.

3.2 Dispersion curve

To elucidate the influence of the resonator's mass and spring within these configurations, the dispersion curve is determined for linear mechanical resonators. A streamlined model, where mechanical damping and the effects of the piezoelectric transducer are neglected (refer to Fig. 1), is employed. In this model, both the stiffness of the monoatomic chain and the resonator are treated as linear. Assuming a harmonic wave solution and incorporating Bloch's theorem, the harmonic displacements of the masses can be expressed as:

$$u_m = u_{m_0} e^{i(G_n a - \omega t)} \tag{4}$$

$$u_r = u_{r_0} e^{i(G_n a - \omega t)}, \tag{5}$$

where u_{m_0} and u_{r_0} are the initial displacements or amplitudes for unit cell or main chain and resonator. Substituting into linear form of Eq. (2) and Eq. (3) results in:

$$m_m m_r \omega^4 - (2k_m m_r(1 - \cos(G_n a)) + k_r m_m$$

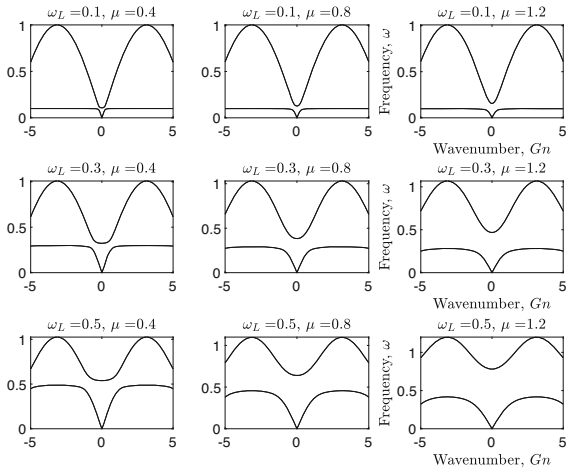

Fig. 2 Dispersion in the periodic structure with varying resonance coupling, and mass ratio. The plots demonstrate the profound influence of resonance conditions on the emergence and width of band gaps, highlighting the potential for tuned wave propagation control by adjusting the μ parameter

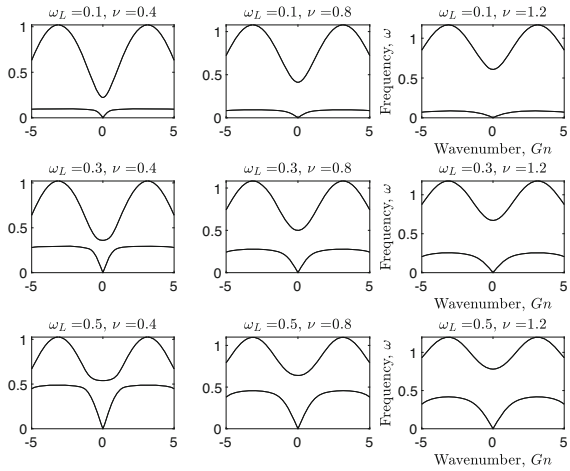

Fig. 3 Dispersion in the periodic structure with varying resonance coupling, and stiffness ratio. The plots demonstrate the profound influence of resonance conditions on the emergence and width of band gaps, highlighting the potential for tuned wave propagation control by adjusting the ν parameter

$$+ k_r m_r)\omega^2 - 2k_m k_r\,(\cos\,(G_n a) - 1) = 0 \tag{6}$$

For wider scope and easy analysis, the normalized dimensionless parameters are defined as follows:

$$\omega_L = \frac{1}{2}\sqrt{\frac{m_m}{k_m}\frac{k_r}{m_r}},\ \mu = \sqrt{\frac{m_r}{m_m}},\ \nu = \sqrt{\frac{k_r}{k_m}},$$
$$\omega_0 = \sqrt{\frac{4k_m}{m_m}} \tag{7}$$

Solving the Eq. (6) produces four roots for ω, which leads to Eqs. (8) and (9) for the individual derivatives with respect to mass and stiffness ratios, μ and ν.

From Figs. 2 and 3, it becomes evident that the properties of the periodic structure are intricately linked with the resonance conditions. One striking observation is that the emergence of a band gap isn't directly associated with a specific wave vector G_n. Instead, it's bound to certain conditions or parameters, possibly hinting at the importance of resonator properties in dictating wave propagation characteristics. This indicates a more complex interplay between the system parameters than just the wave vector, emphasizing the significance of resonator configurations in the system's acoustic properties.

Another pivotal observation is how the width of the band gap is influenced by ν. As the stiffness ratio

$$\omega_{\pm}(k) = \omega_0\sqrt{\frac{1}{2}\left\{\frac{1}{2}[1-\cos(G_n)] + \omega_L^2\left(1+\mu^2\right) \pm \sqrt{4\left(\mu\omega_L^2\right)^2 + \left[\frac{1}{2}[1-\cos(G_n)] + \omega_L^2\left(\mu^2-1\right)\right]^2}\right\}} \tag{8}$$

$$\omega_{\pm}(k) = \omega_0\sqrt{\frac{1}{16}\left\{\sin\left(\frac{G_n}{2}\right)^2 + \frac{1}{4}\nu^2 + \omega_L^2 \pm \sqrt{\left(\frac{1}{4}\nu^2+\omega_L^2\right)^2 + \left(\frac{\nu^2}{4} - 4\omega_L^2\right)\sin\left(\frac{G_n}{2}\right)^2 + \frac{1}{4}\cos(G_n)^2 - \frac{1}{4}}\right\}} \tag{9}$$

The dispersion relation in Eq. (8) emphasizes the effects of μ, profoundly affecting the value of ω at each wave vector G_n. On the other hand, the dispersion relation Eq. (9) focuses more on the stiffness ratio ν, playing a critical role as well in determining the behavior of the system.

becomes more pronounced, the width of the band gap enlarges. This suggests that by manipulating the stiffness of the resonator, one could have a direct influence on the system's acoustic insulation or filtering capabilities. The stronger the coupling, the more formidable

the band gap, acting as a more robust barrier to certain frequency components.

Figure 3 suggests that controlling the system by adjusting ν is a valuable approach. Online tuning with the mass ratio μ can be challenging and impractical, whereas tuning with ν is straightforward, even in real-time scenarios. This holds significant importance for real-time control applications. Changing the mass ratio typically requires halting the operation to physically modify the system-a process that is both time-consuming and may inadvertently alter other critical parameters like the bandgap width. On the other hand, stiffness can be dynamically altered by implementing mechanisms such as actuators that adjust the position of an attached mass on the resonator, facilitating on-the-fly tuning of the bandgap frequency edges without needing to stop the system. This method provides a streamlined and practical solution for tuning the system's acoustic properties in real time, enhancing its adaptability and effectiveness in various applications.

3.3 Linear electromechanical resonators

Electromechanical systems can incorporate piezoelectric components that introduce additional nonlinearity to the system dynamics. These piezoelectric elements serve a dual purpose: they aid in attenuating vibrations within the unit cell, while simultaneously capturing and enhancing energy harvesting in the resonators. With reference to Fig. 1, let's take a scenario where resonators are equipped with piezoelectric elements. This incorporation couples the mechanical motion of the resonators with electrical dynamics, enriching the behavior and capabilities of the system but also complicating its dynamics.

To derive the dynamic equations of the harvester, the Lagrangian formulation for electromechanical systems is employed. The Lagrangian L is defined as:

$$L = T - U + W_e - D \tag{10}$$

Using Lagrange's equation, the governing dynamics are given by:

$$\frac{d}{dt}\frac{\partial L}{\partial \dot{q}_i} - \frac{\partial L}{\partial q_i} + \frac{\partial D}{\partial \dot{q}_i} = Q_i \tag{11}$$

Here, T represents the kinetic energy of the system, U is the potential energy, W_e denotes the coenergy of the piezoelectric module, and D is the dissipative function capturing both mechanical and electrical energy losses.

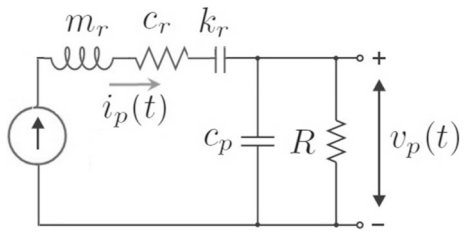

Fig. 4 An equivalent circuit for piezoelectric device model with internal electrode capacitance and load resistance

In this formulation, q_i is the generalized displacement corresponding to a specific degree of freedom in the system. Q_i represents the external force or input acting on the respective degree of freedom. By applying this equation, a set of differential equations governing the behavior of the harvester can be derived, effectively capturing its mechanical and electrical characteristics. The mechanical damping, often referred to as Rayleigh damping, is represented by the term

$$D_m = \frac{1}{2}c_r\,(\dot{u}_r - \dot{u}_m)^2 + \frac{1}{2}c_m\,(\dot{u}_{m^-} - \dot{u}_m)^2 + \frac{1}{2}c_m\,(\dot{u}_m - \dot{u}_{m^+})^2 \tag{12}$$

Piezoelectric devices are often represented by a model where a current source is in parallel with their internal electrode capacitance c_p, as depicted in Fig. 4. Additionally, a simple resistance R is connected to the load in this configuration. The electrical damping arises from the piezoelectric coupling, and it represents the energy dissipation due to electrical losses, denoted by D_p:

$$D_p = \frac{1}{2}\frac{v_p^2}{R} \tag{13}$$

Thus, the total dissipation function for the electromechanical system is given by $D = D_m + D_p$. Considering the piezoelectric transducer integrated into the resonator, the coenergy W_e of the piezoelectric module is given by:

$$W_e = \frac{1}{2}c_p v_p^2 - \theta v_p\,(u_m - u_r) - \frac{1}{2}k_p\,(u_m - u_r)^2 \tag{14}$$

where c_p and k_p denote the equivalent free-body capacitance and stiffness of the piezoelectric element, respectively. θ represents the equivalent force-electric factor of the piezoelectric cantilever beam. The first term corresponds to the electrical coenergy in the capacitance c_p. The second term represents the piezoelectric coenergy. The third term signifies the elastic strain

coenergy in a spring with stiffness k_p. Equatins (11) to (14) detail the electrical behavior of the piezoelectric resonators within the system. It's essential to note that θ and k_p must be experimentally determined to ensure the proposed model aligns with the real setup. In the total mechanical stiffness, $k_r + k_p$, the stiffness contribution from the piezoelectric material, k_p, is significantly smaller in magnitude compared to the resonator's mechanical stiffness, k_r. Therefore, its contribution to mechanical stiffness is often disregarded in the analysis. The energy equations are characterized by linear representations. Given these linear forms of the energy equations, the associated governing equations of motion in metastructure are as follows:

$$\begin{aligned} &m_m\ddot{u}_m(t) + k_m\left(2u_m(t) - u_{m^-}(t) - u_{m^+}(t)\right) \\ &\quad + c_m\left(2\dot{u}_m(t) - \dot{u}_{m^-}(t) + \dot{m}_{m^+}(t)\right) + k_r\left(u_m(t) - u_r(t)\right) \\ &\quad + c_r\left(\dot{u}_m(t) - \dot{u}_r(t)\right) + \theta v(t) = 0 \end{aligned} \tag{15}$$

$$\begin{aligned} &m_r\ddot{u}_r(t) - c_r\left(\dot{u}_m(t) - \dot{u}_r(t)\right) \\ &\quad - k_r\left(u_m(t) - u_r(t)\right) - \theta v(t) = 0 \end{aligned} \tag{16}$$

$$c_p\dot{v_p}(t) + \frac{v_p(t)}{R} - \theta(\dot{u}_m(t) - \dot{u}_r(t)) = 0 \tag{17}$$

Equations (15) to (17) are included with multiple parameters, adding to their complexity. For enhanced clarity and broader applicability, the model's governing equations are recast using the established normalized parameters as follows:

$$\begin{aligned} &\ddot{u}_m(t) + 4\zeta_m\omega_m\dot{u}_m(t) - 2\zeta_m\omega_m\left(\dot{u}_{m^-}(t) + \dot{u}_{m^+}(t)\right) \\ &\quad + 2\omega_m^2 u_m(t) - \omega_m^2(u_{m^-}(t) + u_{m^+}(t)) \\ &\quad + 2\mu\zeta_r\omega_r\left(\dot{u}_m(t) - \dot{u}_r(t)\right) + \nu^2\omega_m^2\left(u_m(t) - u_r(t)\right) \\ &\quad + k_e^2\nu^2\omega_m^2\bar{v}(t) = 0, \end{aligned} \tag{18}$$

where for the last mass $u_m(t) - u_{m^+}(t) = 0$, $\dot{u}_m(t) - \dot{u}_{m^+}(t) = 0$, and for the first mass $u_{m^-}(t) = u_b(t)$. The equation for the resonator becomes:

$$\begin{aligned} &\ddot{u}_r(t) - 2\zeta_r\omega_r\left(\dot{u}_m(t) - \dot{u}_r(t)\right) \\ &\quad - \omega_r^2\left(u_m(t) - u_r(t)\right) - k_e^2\omega_r^2\bar{v}(t) = 0 \end{aligned} \tag{19}$$

Lastly, the equation representing the piezoelectric effect is given as:

$$\dot{\bar{v}}(t) + \frac{\omega\dot{\bar{v}}(t)}{r_g} - (\dot{u}_m(t) - \dot{u}_r(t)) = 0 \tag{20}$$

where $k_e^2 = \theta^2/\left(c_p k_r\right)$ indicates the electromechanical coupling coefficient, $\bar{v} = c_p v_p/\theta$ is the scaled piezoelectric output voltage, and $r_g = Rc_p\omega_r$ designates the proportion of the actual load R to its optimal value R_{opt}. Additionally, $\zeta_m = c_m/(2m_m\omega_m)$ and $\zeta_r = c_r/(2m_r\omega_r)$ are the damping ratios of the main chain and the resonator, respectively. Furthermore, $\nu^2 = k_r/k_m$ represents the stiffness proportion between the resonator and the chain mass, while $\mu = m_r/m_m$ depicts the mass ratio between the resonator and the chain mass.

3.4 Analysis of power output of standard piezoelectric circuit for energy harvesting

The primary objective of this research is to investigate the inherent properties of various types of nonlinearity in piezoelectric materials, rather than comparing different circuit models. For a consistent evaluation, every type of nonlinearity is paired with the same standard circuit, ensuring each nonlinearity is studied in isolation and without the influence of varying circuit efficiencies. A standard rectifier interface circuit with no electrical losses for energy harvesting is explored using a lumped parameter model. In design analysis for energy harvesting, a simplified circuit is frequently employed, as shown Fig. 5. In this configuration, the regulation circuit and battery are substituted with an equivalent resistor labeled as R, and the rectified voltage across it is denoted as v_e. It is assumed, for the purposes of this study, that the rectifying bridge is in an ideal and faultless state. A rectifying bridge circuit is integrated, targeting a stable output DC voltage v_e, which connects the load directly. It is assumed that the filter capacitor c_e is sufficiently large to render v_e essentially constant. In steady-state operation, the average rectified voltage and displacement are related. Governed by equations, the piezo voltage $v_p(t)$ is proportional to the displacement $u(t)$. Both variables are modeled as $u(t) = u_0\sin(wt-\theta)$ and $v_p(t) = v_{p_0}(wt-\theta)$, where u_0 is the constant displacement magnitude, and $v_{p_0}(t)$ is a periodic function with $|v_{p_0}(t)| \le v_e$.

During a semi-period $\frac{T}{2}$, defined as $T = \frac{2\pi}{w}$, the integral of the rate of change of $v_p(t)$ is $2v_e$. This yields

$$\int_{t_1}^{t_2} I(t)dt = \frac{T}{2}\frac{v_e}{R}, \tag{21}$$

delineating the relationship between the current and average rectified voltage [38]. The integral $\int_{t_1}^{t_2}\dot{v}_p(t)dt$ represents the total change in the piezoelectric voltage $v_p(t)$ from time t_1 to t_2. If $v_p(t)$ oscillates between $-v_e$ and v_e during this semi-period $\frac{T}{2}$, then the total change in $v_p(t)$ is $v_e - (-v_e) = 2v_e$. If $u(t)$ is oscillating from its minimum $-u_0$ to its maximum u_0 during the semi-period from time t_1 to t_2, then the change in $u(t)$ during this period is $u_0 - (-u_0) = 2u_0$.

Assuming the standard linear form and rewriting Eq. (17) yields to:

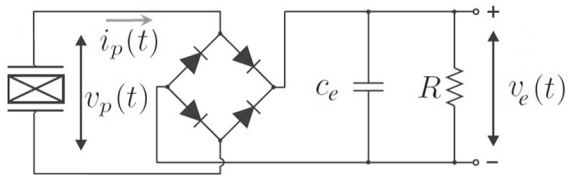

Fig. 5 Classical energy harvesting circuit for the standard electronic interfaces

$$c_p \dot{v}_p(t) + i_p(t) = \theta \dot{z}(t), \tag{22}$$

where $z(t)$ is the relative displacement of the mass chain with respect to the resonator in each unit cell. Integration of Eq. (22) from time t_1 to t_2 gives:

$$2c_p v_e + \frac{T}{2}\frac{v_e}{R} = 2\theta z_0 \tag{23}$$

This equation correlates the changes in stored electric charge, current, and mechanical displacement between times a and b. Given $\frac{T}{2} = \frac{\pi}{\omega}$, the equation for v_e expressed as:

$$v_e = \frac{R\theta\omega}{Rc_p\omega + \frac{\pi}{2}} z_0 \tag{24}$$

Furthermore, the average harvested power P can be well-defined as:

$$P = \frac{v_e^2}{R} = \frac{R\theta^2\omega^2}{\left(Rc_p\omega + \frac{\pi}{2}\right)^2} z_0^2 \tag{25}$$

3.5 Nonlinear electromechanical resonators

The behavior of a linear piezoelectric element is described by Eq. (17). While linearized models offer simplicity and are often adequate for many applications, they may miss critical behaviors and limit our understanding and predictive capabilities. The study of nonlinearity provides a comprehensive and accurate view of systems, essential for both practical applications and scientific inquiry. When introducing any of these nonlinearities into the model, it is essential to ensure that they are grounded in physical reality or experimental observations relevant to the system. Modeling choices should be justified based on the underlying physics, empirical data, or both.

One common approach to introduce nonlinearity is by using a polynomial expansion. When considering the piezoelectric response, one possibility is a nonlinear dependency of the voltage, denoted as $v(t)$, on strain. Adding a simple quadratic nonlinearity to the piezoelectric equation, yields to:

$$c_p \dot{v}(t) + \frac{v(t)}{R} - \theta\left(\dot{u}_m(t) - \dot{u}_r(t)\right) - \beta\left(\dot{u}_m(t) - \dot{u}_r(t)\right)^2 = 0 \tag{26}$$

where β is a coefficient of the nonlinear term. In this model, the piezoelectric response starts to deviate from linearity as the strain (differential displacement) increases. The term β dictates the strength of this nonlinearity. If β is zero, the system returns to the original linear behavior. In electronic circuits, transistors, especially MOSFETs, can exhibit polynomial behavior with respect to gate-source voltage and drain current, leading to nonlinear amplification. Moreover, the dynamics of robotic arms can have nonlinear components due to joint friction, and these can be represented as polynomial functions of velocities.

Upon introducing nonlinearity, the system can be numerically simulated using techniques tailored for nonlinear differential equations, such as the Runge–Kutta method. Software packages, like MATLAB's Simulink or COMSOL, can also be employed. Initial conditions and boundary conditions need to be established based on the specific study.

Apart from polynomial expansion, there are several other types to introduce and study nonlinearity in a piezoelectric energy harvester.

3.6 Theoretical models for the nonlinear energy harvesting

The nonlinear behavior in energy harvesting can be succinctly captured in a generalized equation which encompasses multiple facets of nonlinearity. Consider the following expression:

$$\alpha\frac{v(t)}{R(\omega)} + c_p\frac{d}{dt}[f(v(t))] - \theta\left[g\left(\frac{d^2}{dt^2}u_m(t) - \frac{d^2}{dt^2}u_r(t), v(t)\right)\right] - h\left(\int v(t)dt\right) = 0 \tag{27}$$

Here: $R(\omega)$ introduces nonlinearity as a function of frequency. Adjustable parameter, α can be varied to explore different system behaviors and regimes. $f(v(t))$ introduces nonlinearity as a function of the voltage across the impedance.

The term $g\left(\frac{d^2}{dt^2}u_m(t) - \frac{d^2}{dt^2}u_r(t), v(t)\right)$ represents a nonlinear function of the acceleration and voltage. $h\left(\int v(t)dt\right)$ is the nonlinearity introduced by an integral of voltage over time. It is important to note that this is a completely abstract and generalized equation that must be determined based on the system specifications and the physics involved.

The Eq. (27) exemplifies a multi-faceted nonlinear system that integrates various nonlinear dependencies into a comprehensive framework. $R(\omega)$ denotes a frequency-dependent nonlinearity, reflective of materials like semiconductors or piezoelectric elements under resonance. $f(v(t))$ embodies a voltage-dependent nonlinearity, typical in devices like diodes or transistors, where shifting voltage can alter operational regimes. The term $g\left(\frac{d^2}{dt^2}u_m(t) - \frac{d^2}{dt^2}u_r(t), v(t)\right)$ encapsulates a coupled nonlinearity, hinting at a complex relationship between the accelerations of two system components and voltage. Lastly, $h\left(\int v(t)dt\right)$ introduces a memory effect, capturing historical influences on the system, akin to hysteresis or capacitive responses.

To derive the standard linear form of a piezoelectric equation, the resistance is considered as not frequency-dependent, and the capacitance is assumed not to be influenced by voltage variations, simplifying the term $c_p\frac{d}{dt}[f(v(t))]$ to $c_p\dot{v}(t)$ by setting $f(v(t)) = v(t)$. The electromechanical coupling is taken to be linear, meaning the term with $g(\cdot)$ reduces to $\theta\left(\dot{u}_2(t) - \dot{u}_1(t)\right)$, indicating the coupling coefficient isn't influenced by displacement, velocity, or acceleration. Lastly, the term $h\left(\int v(t)dt\right)$ is disregarded, signifying that the integral of voltage over time does not significantly influence the system dynamics. Under these assumptions and simplifications, the generalized Eq. (27) reduces to Eq. (17), which is the standard linear form of a rectifier circuit.

3.7 Internally coupled resonators with mechanical nonlinearity

To clarify the dynamics within the mechanically internally coupled system, the analysis strategically simplifies the system by focusing exclusively on the springs, omitting damping effects and electromechanical elements. This approach allows for a concentrated examination of the system's behavior under the influence of linear springs in the primary chain and resonators, alongside nonlinear springs that facilitate internal coupling between resonators. As depicted in Fig. 6, the

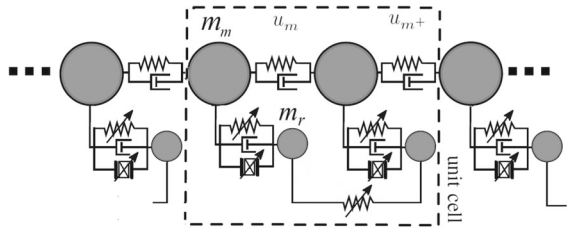

Fig. 6 Nonlinear mechanical internally coupled chain. The dashed rectangle is unit cell

system consists of a nonlinear mechanical internally coupled chain, with the unit cell highlighted by the dashed rectangle. Consequently, the dynamic behavior of the system will be primarily dictated by this nonlinear internal coupling between resonators, even as the rest of the system retains its linearity. This configuration allows for a focused study on the impacts and potential advantages of having a nonlinear inter-resonator spring in an otherwise linear spring system.

The kinetic energy, denoted by T, encompasses the motion of the main chain and the resonators and is given by:

$$T = \frac{1}{2}m_m\left(\dot{u}_m^2 + \dot{u}_{m^+}^2\right) + \frac{1}{2}m_r\left(\dot{u}_r^2 + \dot{u}_{r^+}^2\right) \tag{28}$$

The potential energy, represented by U, captures the energy stored in the main chain's linear springs, the coupling springs between the main chain and resonators, and the nonlinear internal coupling springs of the resonators:

$$\begin{aligned} U =& \frac{1}{2}k_m\left[(u_{m^-} - u_m)^2 + (u_m - u_{m^+})^2 + (u_{m^+} - u_{m^{++}})^2\right] \\ &+ \frac{1}{2}k_r\left[(u_m - u_r)^2 + (u_{m^+} - u_{r^+})^2\right] \\ &+ \frac{1}{2}k_{c_1}(u_r - u_{r^+})^2 + \frac{1}{4}k_{c_2}(u_r - u_{r^+})^4 \end{aligned} \tag{29}$$

Here, k_{c_1} and k_{c_2} are the linear and nonlinear coupling coefficients, respectively. The k_{c_1} term introduces a linear coupling between resonators, while k_{c_2} induces a bistable nonlinearity due to its quartic nature between resonators. When both k_{c_1} and k_{c_2} are positive $\left(k_{c_1} > 0\right.$ and $\left.k_{c_2} > 0\right)$, a classic monostable state is achieved, simplifying the system by avoiding the necessity to find and linearize around a stable point. This selection, while ensuring straightforward and stable system behavior, is often employed to eschew the complexities that arise when dealing with bistable systems, particularly when $k_{c_1} < 0$ and $k_{c_2} > 0$.

Utilizing the Lagrangian formulation, the system's equations of motion are derived as:

$$m_m \ddot{u}_m(t) + k_m \left(2u_m(t) - u_{m^-}(t) - u_{m^+}(t)\right) + k_r \left(u_m(t) - u_r(t)\right) = 0 \quad (30)$$

$$m_r \ddot{u}_r(t) - k_r \left(u_m(t) - u_r(t)\right) + k_{c_1} \left(u_r(t) - u_{r^+}(t)\right) + k_{c_2} \left(u_r(t) - u_{r^+}(t)\right)^3 = 0 \quad (31)$$

$$m_m \ddot{u}_{m^+}(t) + k_m \left(2u_{m^+}(t) - u_m(t) - u_{m^{++}}(t)\right) + k_r \left(u_{m^+}(t) - u_{r^+}(t)\right) = 0 \quad (32)$$

$$m_r \ddot{u}_{r^+}(t) - k_r \left(u_{m^+}(t) - u_{r^+}(t)\right) - k_{c_1} \times \left(u_r(t) - u_{r^+}(t)\right) - k_{c_2} \left(u_r(t) - u_{r^+}(t)\right)^3 = 0 \quad (33)$$

The superscript '$^+$' indicates the two adjacent mass-in-mass structures, where $u_{m^{++}}$ denotes the displacement of the mass or unit that is two positions away from mass m. Utilizing Bloch's theorem, the waveform of the harmonic displacements of masses can be expressed as:

$$\begin{aligned} u_m &= u_{m_0} e^{i(G_n x - \omega t)} \\ u_{m^+} &= u_{m_1} e^{i(G_n x + G_n a - \omega t)} \\ u_r &= u_{r_0} e^{i(G_n x - \omega t)} \\ u_{r^+} &= u_{r_1} e^{i(G_n x + G_n a - \omega t)}, \end{aligned} \quad (34)$$

where G_n represents the wave number or spatial frequency, dictating the spatial periodicity of the wave over the unit cell with the dimension of a. The coefficients $u_{m_0}, u_{m_1}, u_{r_0}$, and u_{r_1} represent the complex wave amplitudes. Integrating these terms into the provided equations leads to the derivation of the dispersion relation. The associated matrix is determined for this purpose, and by setting its determinant to zero, a relationship between G_n and ω is established. For nonlinear scenarios, as presented in the above equations, a numerical approach is typically employed. From four inertias in a unit cell, an eighth-order dispersion equation arises when the determinant is zero. This results in four curves with three band gaps on the positive real axis, indicating that internally coupled metamaterials offer additional band gaps over conventional ones.

In this study, we focus on a specific frequency range. A comprehensive analysis of the effects of piezoelectric nonlinearities across the entire frequency spectrum is beyond the scope of this work.

3.8 Electromchanical internally coupled resonators

In the previous sections, we explored metamaterials with internal resonator coupling. Given the challenges associated with designing and implementing the internal spring, especially when targeting negative stiffness, an alternative approach is to employ an electrical shunt circuit. Specifically, a prototype capacitance can mimic the behavior of a mechanically internally coupled resonator.

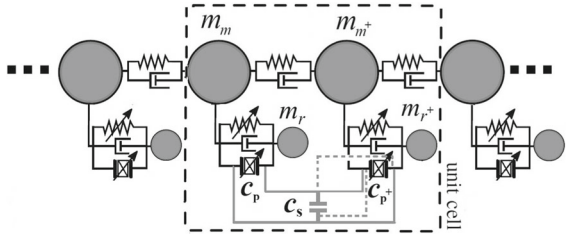

Fig. 7 Internally coupled with electrical shunt circuit. Forward (dash) and reverse (solid) capacitance shunting configuration

3.8.1 Internal coupling via shunt capacitance circuit technique

In this section, the shunt capacitance circuit technique is employed to model a two-degree-of-freedom electrical system with internal coupling, as illustrated in Fig. 7. In this scenario, capacitance is incorporated as a key component instead of utilizing the previously formulated resistance (R).

Figure 7 presents two different configurations of the shunt circuit: the forward and the reverse. For the forward setup, the top and bottom surfaces of the piezoelectric transducer on the left align with the analogous surfaces of its counterpart on the right. Conversely, the reverse configuration has the top and bottom surfaces of the two piezoelectric transducers connected in an opposite fashion. In both setups, a capacitor is connected in parallel to both piezoelectric transducers.

The analytical procedures for both configurations are analogous, leading to comparable conclusions. The distinction in circuit connectivity between these two setups only results in a sign reversal in the ultimate expression for equivalent coupling stiffness. Both forward and reverse connections can achieve the same functionality, albeit with differing capacitance tuning strategies. This investigation primarily focuses on the reverse connection configuration. In its absence of external capacitance, it exhibits characteristics akin to a standard spring with positive stiffness, simplifying its interpretation in an equivalent mechanical context.

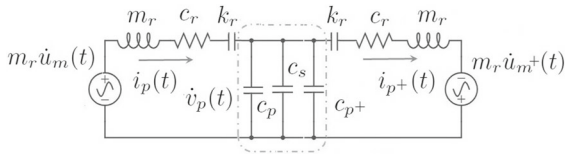

Fig. 8 Equivalent electrical system representation of the unit cell resonators with capacitance shunt circuit using the impedance analogy

Capacitance typically relates the change in electric charge to shifts in electric potential. With positive total capacitance, a discharge of current leads to a voltage decrease across the capacitor, whereas with negative total capacitance, the voltage increases. Utilizing the impedance analogy (current to velocity, charge to displacement, voltage to force), the circuit segments LRC and LRC^+ correspond to the resonators $m_r c_r k_r$ and $(m_r c_r k_r)^+$, respectively, as illustrated in Fig. 8. For simplicity, the mechanical properties of the resonators (mass, stiffness, and damping) are assumed to be identical.

The voltage across the total capacitance represents the force interaction between these resonators. Additionally, the current through total capacitance, representing the difference in currents in the loops' paths, indicates the difference in velocity between the resonators. The charge variation in total capacitance indicates the displacement difference between the resonators. Hence, the capacitor in the electrical system can be envisioned as a spring, k_s coupling the resonators in the mechanical domain, with positive total capacitance acting as a positive-stiffness coupling spring and negative total capacitance as a negative-stiffness spring.

Considering the reversed configuration of the two piezoelectric transducers, the voltages exhibit identical magnitudes but with opposite directions. Factoring in the current passing through the parallel-connected capacitance c_s, the relationship between the voltages is expressed as:

$$\frac{1}{c_s}\int \left(i_p(t) - i_{p^+}(t)\right) dt = v_p(t) \tag{35}$$

The design employs an internal shunt capacitance circuit to optimize the band gap behavior in resonators. When this capacitance acts as a negative capacitor and is finely tuned, it can offset the capacitances of linked piezoelectric transducers, enhancing the coupling between adjacent resonator.

Considering damping in the resonators and assuming identical stiffness, damping coefficients, and masses for all resonators, the governing equations for the motion of the two resonators within a unit cell (refer to Fig. 7) relative to the mass of the chain is as follows:

$$\begin{aligned} &m_r\ddot{z}_r(t) + c_r\dot{z}_r(t) + k_r z_r(t) + \theta_r v_p(t) \\ &\quad = m_r\ddot{u}_m(t) \end{aligned} \tag{36}$$

$$\begin{aligned} &m_r\ddot{z}_{r^+}(t) + c_r\dot{z}_{r^+}(t) + k_r z_{r^+}(t) + \theta_{r^+} v_{p^+}(t) \\ &\quad = m_r\ddot{u}_{m^+}(t) \end{aligned} \tag{37}$$

The relative displacements of these resonators with respect to the main chain structure are denoted by $z_r(t)$ and $z_{r^+}(t)$. The electromechanical coupling coefficients are θ_r and θ_{r^+}, and the voltages across the corresponding piezoelectric transducers are $v_p(t)$ and $v_{p^+}(t)$. The excitation displacements are represented as $u_m(t)$ for the left and $u_{m^+}(t)$ for the right resonators.

The governing electrical domain equations for the piezoelectric transducers are as follows:

$$c_p\dot{v}_p(t) + i_p(t) - \theta_r\dot{z}_r(t) = 0 \tag{38}$$

$$c_{p^+}\dot{v}_{p^+}(t) + i_{p^+}(t) - \theta_{r^+}\dot{z}_{r^+}(t) = 0 \tag{39}$$

By substituting Eq. (35) into Eqs. (38) and (39), expressions for currents $i_p(t)$ and $i_{p^+}(t)$ in the loops are derived as:

$$i_p(t) = \frac{c_{p^+}\theta_r\dot{z}_r + c_p\theta_{r^+}\dot{z}_{r^+} + c_s\theta_r\dot{z}_r}{c_p + c_{p^+} + c_s} \tag{40}$$

$$i_{p^+}(t) = \frac{c_{p^+}\theta_r\dot{z}_r + c_p\theta_{r^+}\dot{z}_{r^+} + c_s\theta_{r^+}\dot{z}_{r^+}}{c_p + c_{p^+} + c_s} \tag{41}$$

Substituting Eqs. (40) and (41) into Eq. (35) and integrating with respect to time for zero initial condition yields:

$$v_p(t) = \frac{(\theta_r z_r - \theta_{r^+} z_{r^+})}{c_p + c_{p^+} + c_s} \tag{42}$$

$$v_{p^+}(t) = -\frac{(\theta_r z_r - \theta_{r^+} z_{r^+})}{c_p + c_{p^+} + c_s} \tag{43}$$

After substituting Eqs. (40) and (41) into Eq. (35) and integrating with respect to time, assuming θ_r is equal to θ_{r^+}, the equations of motion can be simplified as follows

$$\begin{aligned} &m_r\ddot{z}_r(t) + c_r\dot{z}_r(t) + k_r z_r(t) \\ &\quad + k_s\left(z_r(t) - z_{r^+}(t)\right) = m_r\ddot{u}_m(t) \end{aligned} \tag{44}$$

$$\begin{aligned} &m_r\ddot{z}_{r^+}(t) + c_r\dot{z}_{r^+}(t) + k_r z_{r^+}(t) \\ &\quad - k_s\left(z_r(t) - z_{r^+}(t)\right) = m_r\ddot{u}_{m^+}(t), \end{aligned} \tag{45}$$

where

$$k_s = \frac{\theta_r^2}{c_p + c_{p^+} + c_s}. \tag{46}$$

Implementing coupling through piezoelectric transducers and a shunt capacitance circuit is practical, as it serves as an equivalent spring that relates the motions of two resonators via their relative displacements. This coupling mechanism, resulting from local resonances, creates additional band gaps in metamaterials by generating two resonant frequencies.

The piezoelectric transducers, when shunted, act as an analogous internal coupling spring k_s, similar to the mechanical internal coupling that links the movement of two resonators. However, it's important to note that using a negative shunt capacitor, which is a type of positive feedback in op-amp circuits, can increase the risk of system instability without the right parameter choices. Despite this, the design's strength is its tunability and ability to generate multiple band gaps, offering robust vibration suppression.

3.9 Stability analysis

The behavior of the system is largely determined by the parameter k_s, which characterizes the stiffness introduced due to electromechanical coupling via the shunt circuit. To introduce negative stiffness, assuming electromechanical coupling, θ_r is equal to θ_r^+, it is requisite that k_s be negative. This can be expressed mathematically as:

$$k_s = \frac{\theta_r^2}{c_p + c_{p^+} + c_s} < 0 \tag{47}$$

Given that θ_r^2 will always be positive, the denominator must be negative for k_s to be negative. Thus, either c_p and/or c_{p^+}must be negative (which could signify negative capacitance introduced, for instance, by an active circuit) while the magnitude of their sum should be greater than c_s.

Utilizing the Jacobian method and employing the vector $[z_r(t), z_{r^+}(t)]$ for the linear matrix of the system depicted by Eqs. (44) and (45), the eigenvalues are provided as $\lambda_{1,2} = \pm\frac{\sqrt{-k_r m_r}}{m_r}$, and $\lambda_{3,4} = \pm\frac{\sqrt{-m_r(k_r+2k_s)}}{m_r}$. The stability of a system is contingent upon the real parts of its eigenvalues. For the system at hand, when $k_r + 2k_s > 0$, all eigenvalues are purely imaginary, suggesting marginal stability. In this scenario, the system, when perturbed, will oscillate indefinitely without growing unbounded or decaying to zero. Conversely, when $k_r + 2k_s < 0$, the system presents two positive eigenvalues and two negative ones. The presence of positive real eigenvalues clearly indicates an unstable system. This underscores the paramountcy of the interplay between the resonator's spring constant and the feedback shunt capacitance stiffness (associated with k_s). If the feedback's influence is excessively robust and negative, it could push the system into an unstable regime. Therefore, for a stable system, the criterion for c_s is:

$$c_s > \frac{8m_r\theta_r^2}{c_r^2 - 4k_r m_r} - c_p - c_{p^+} \tag{48}$$

For most practical applications, a strictly stable system, where all disturbances decay, is more desirable than a marginally stable one. Exploring stability in lumped parameter systems reveals that maintaining a strictly stable condition, preferable for practical applications, hinges on a fine balance within the system's parameters, as indicated by the derived criterion. For a detailed examination of stability analysis and energy harvesting within lumped parameter systems, particularly those incorporating internally coupled resonators, the study in [39] extends the discussion to encompass a variety of conditions.

4 Simulation analysis and discussion

The behavior of the proposed models is observed through simulations using the case study parameters outlined in Table 1. The system model was developed by formulating a set of interconnected ordinary differential equations that encapsulate both the mechanical and electrical dynamics of the piezoelectric harvesters. Numerical solutions to this system were obtained utilizing the fourth-order Runge–Kutta method with a carefully chosen time step to guarantee precision and stability in the results. The simulation results explore various aspects of the system's dynamic response, including vibration mitigation, energy harvesting, power output, and robustness analysis.

4.1 Nonlinear mechanical resonators and internal coupling dynamics

In Fig. 9, the band gap behaviors for various system configurations are presented. The system's natural fre-

Table 1 Defined parameters for the piezoelectric model

Parameter	Value
Mass of main chain (m_m)	0.056 kg
Mass of resonator (m_r)	0.0336 kg
Spring constant of main chain (k_m)	150 N/m
Spring constant of resonator (k_r)	129.6 N/m
Damping coefficient of main chain (c_m)	0.0464 Ns/m
Damping coefficient of resonator (c_r)	0.0334 Ns/m
Piezoelectric capacitance (c_p)	1.5 mF(C/m)
Electromechanical coupling coefficient (θ)	0.25 N/V
Nonlinear stiffnesses quadratic coefficient (γ_2)	-500 N/m^2
Nonlinear stiffnesses cubic coefficient (γ_3)	15000 N/m^3
Linear coupling coefficient (k_{c_1})	198(-20) N/m
Nonlinear coupling coefficient (k_{c_2})	2386(880) N/m^3
Shunt capacitance (c_s)	-7.9 mF(C/m)
Internal resistance (R)	500 Ω

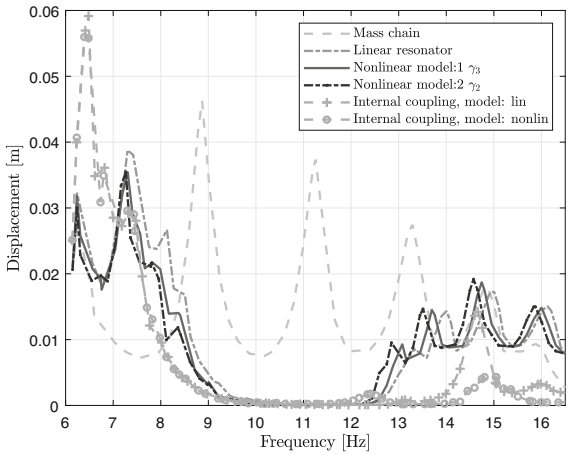

Fig. 9 Comparative analysis of band gap behaviors in a 1-D chain system: insights from linear, nonlinear, and internally coupled resonator configurations

quencies are analyzed within a range from 6 to 17 Hz. The introduction of locally resonating elements distinctly establishes a band gap, differentiating these configurations from the conventional metastructure setup. This band gap characteristic is attributed to the linear local resonance, which undergoes out-of-phase motion when subjected to an external excitation frequency near its local resonance frequency.

The nonlinear analysis focuses primarily on contrasting linear systems with their nonlinear counterparts, in addition to examining internally coupled sys-

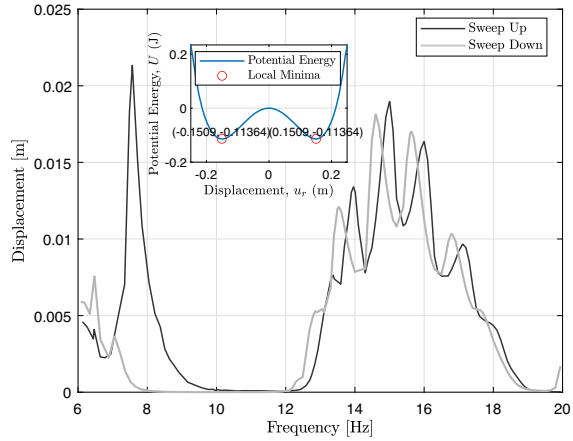

Fig. 10 Displacement response of bistable nonlinear mechanical internal coupling resonators. Linear coupling coefficient $k_{c_1} = -20$ N/m, and nonlinear coupling coefficient $k_{c_2} = 880$ N/m^3. Inset: Resonator's potential energy profile for the specified coupling parameters

tems. Effects arising from bifurcation and its influence on frequency sweeps are not explored in this context. Nonlinear resonators, both quadratic and cubic, exhibit a more extensive band gap compared to their linear counterparts. For the quadratic nonlinearity, a modified relation is employed:

$$f_r = k_r u + \gamma_{r_2} u|u| \tag{49}$$

This model facilitates numerical simulations and provides a comparative benchmark against cubic nonlinearities. Both linear and nonlinear internal coupling serve to effectively increase the bandgap within the main chain, as illustrated in Fig. 9. The analysis of mechanical internal coupling reveals that linear and nonlinear internal couplings may not necessarily boost power and energy generation, even when the main chain has a wider bandgap. Surprisingly, energy harvested with internal coupling is sometimes lower than in a single-chain setup. This suggests that interactions between resonators could hinder energy accumulation.

Figure 10 shows the transmission response of a metastructure equipped with a nonlinear bi-stable internal coupling resonator. The observed bifurcation is shaped by linear ($k_{c_1} = -20$ N/m) and nonlinear ($k_{c_2} = 880$ N/m^3) coupling coefficients, with the continuous sweep offering a detailed system response. The main graph underlines the system's potential energy dynamics, with an unstable origin indicating negative stiffness. This complexity is further highlighted by bifurcations between 14–16 Hz. The inset reveals var-

ious energy states the system can attain. Multiple local minima suggest system multi-stability, especially during large fluctuations. Hysteresis is evident from discrepancies in sweep traces, particularly in lower frequencies from 6 Hz and 10 Hz. However, it's vital to understand the intent behind the choice of parameters in this study. The deliberate restriction to a specific frequency range serves to mimic negative stiffness phenomena observed in specific electromechanical systems.

Cubic nonlinearities, with their symmetric properties, are observed to manifest either pure hardening or softening behaviors. This stands in contrast to the dual behavior inherent to asymmetric quadratic nonlinearities. The significance of optimal impedance matching is underscored, highlighting its role in achieving enhanced vibration suppression and energy harvesting. However, as theoretical constructs transition to tangible systems, certain compromises are often necessary to accommodate weakly and strongly coupled systems [34,40].

Setting both k_{c_1} and k_{c_2} to be positive (see Table 1) induces a classic monostable state, simplifying the system and avoiding the complications inherent in managing bistable systems, particularly when $k_{c_1} < 0$ and $k_{c_2} > 0$.

Furthermore, when evaluating mechanically internal coupling configurations, there is a discernible decrease in efficiency for energy harvesting. While band gaps are inherent features of these systems, they may sometimes present challenges, especially in terms of wave propagation. The compounded presence of a band gap and internal coupling appears to negatively impact overall energy output. Detailed investigations into the dynamics of these coupled resonators could provide deeper insights into the underlying mechanisms that result in reduced efficiency.

Nonetheless, simulating internally coupled resonators with bistable nonlinearity to observe bifurcation effects was considered valuable. However, due to the inherent complexity and the desire to avoid simulating rapid transitions, this approach was ultimately avoided.

Figure 11 shows the nonlinear spring force-displacement relation for cubic nonlinearities, and transmittance of this nonlinearity. It shows the influence of cubic nonlinearity in the system. Distinctly, the nonlinearity is characterized by the coefficient γ_3, where its sign determines the hardening or softening

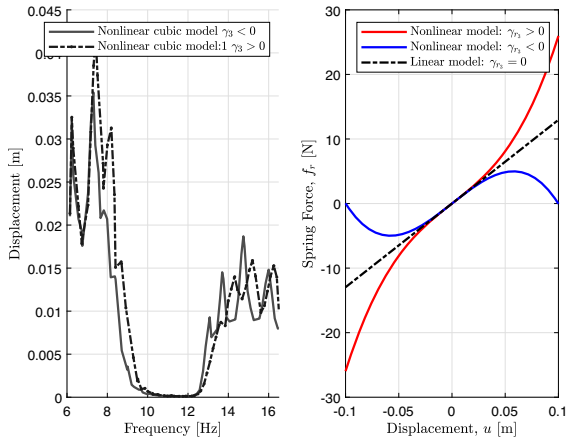

Fig. 11 Nonlinear characteristics of the 1-D chain system: **a** Transmittance response influenced by cubic nonlinearity, and **b** nonlinear spring force-displacement relationship for cubic nonlinearities

nature of the system. For the resonator's equation force:

$$f_r = k_r u + \gamma_{r_3} u^3, \tag{50}$$

The value of γ_{r_3} has been varied as $\pm 15000\ \mathrm{N/m^3}$, pointing to two contrasting behaviors. When $\gamma_{r_3} > 0$, the system exhibits hardening nonlinearity. This means as the amplitude of excitation increases, the natural frequency of the system also escalates. Conversely, for $\gamma_{r_3} < 0$, we observe a softening nonlinearity. Here, an increase in the excitation amplitude leads to a decrease in the system's natural frequency. To reduce the complexity of the system, bistable nonlinearity is deliberately avoided, eliminating the need to perform up and down-frequency simulations. In the broader context, the introduction of diatomic chains, incorporation of nonlinear local resonators (as depicted in Figs. 6, 7), or a transition to 2D setups, allows for deeper exploration and comprehension of the intricate nonlinear phenomena in advanced systems. Building on the findings from the frequency domain analysis, it becomes evident in the time domain that systems with cubic nonlinearity commence vibration suppression earlier compared to those with linear resonators. The duration during which effective suppression occurs depends on multiple factors, including the natural frequency of the system and its inherent physical properties.

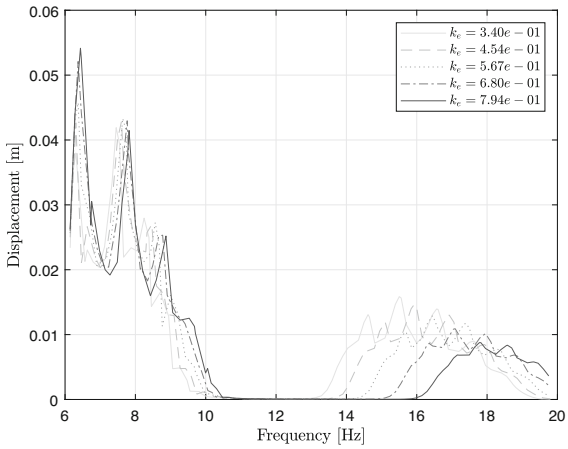

Fig. 12 Band gap illustration for a monochain featuring linear local resonators with $n = 8$ mass chains, demonstrating the influence of k_e on band gap and metastructure response

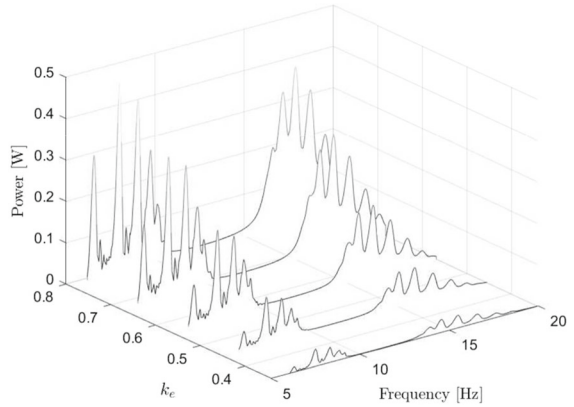

Fig. 13 Electromechanical coupling's impact on energy harvesting: illustration of the power harvested across varying k_e in an $n = 8$ unit cell monochain, showcasing the pivotal role of the electromechanical coupling coefficient in optimizing energy conversion and system dynamics

4.2 Investigation on energy harvesting performance in linear electromechanical metamaterial

In Fig. 12, the transmittance for various values of k_e, representing the piezoelectric coupling coefficient (Eq. 20), is depicted. For the analysis, the stiffness of the piezoelectric element, represented by k_p, is considered negligible compared to the significantly greater stiffness of the resonator, denoted by k_r. This simplification enables a focus on the effects of other parameters without the interference of k_p.

A noticeable broadening of the band gap is observed as the electromechanical coupling coefficient k_e is increased, indicating an enhanced capacity of the system to suppress vibrations. The peaks of the transmittance adjacent to this band gap are notably sensitive to variations in k_e, while those further from the band gap show minimal alternations. This observation emphasizes the crucial role played by k_e in modulating the system's response when using piezoelectric materials, highlighting its significant contribution to vibration control in complex systems. Additionally, the parameter r_g, defined as $r_g = \omega_r c_p R$, can be adjusted to achieve minimal transmittance at each frequency.

As depicted in Fig. 13, the electromechanical coupling coefficient k_e, plays a pivotal role in the energy harvesting performance of a system comprising eight unit cells. This parameter k_e, essentially governs how efficiently piezoelectric materials convert mechanical energy to electrical energy and vice versa, exerting a significant influence on the outcomes of energy harvesting. In scenarios characterized by weak coupling, an increase in k_e results in a notable increase in power output. Conversely, in situations involving strong coupling, an increase in k_e leads to a power level that remains constant, preventing any additional improvements. For our subsequent analysis, a weak coupling value of $k_e = 0.567\,(c_p = 1.5\text{mF})$ is selected to avoid the complex power response patterns observed in strong coupling situations. To comprehensively assess overall energy harvesting performance, we uniformly adjust the resistors R, connected to the piezoelectric transducers, and consolidate power outputs from these resistors. High-capacitance (millifarad-level) piezoelectric materials have a wide range of applications, from energy-harvesting floor tiles in busy areas to vibration damping in machinery, structural monitoring, energy recapture in vehicle suspensions, self-charging personal electronics, and power sources for wearable health monitors. To enhance the capacitance of these materials, strategies include selecting materials with higher dielectric constants, optimizing element geometry, using multi-layer structures, and parallel capacitor configurations, aiming to boost energy harvesting capabilities and efficiency in diverse applications.

5 Nonlinear electromechanical models

This section examines the dynamics of nonlinear electromechanical models, essential for advancing energy

harvesting systems. Various nonlinear phenomena are examined to reveal their significant impact on the performance of piezoelectric devices. By elucidating the interactions between mechanical and electrical components, these nonlinear models demonstrate potential for optimizing energy conversion.

5.1 Model NL: 1-polynomial nonlinearity in resonators

Polynomial nonlinearity finds practical applications in electronic circuits with diodes and in thermostats or temperature controllers. In diodes, the voltage-dependent behavior transitions from an open switch to a closed switch as voltage crosses a threshold, using piecewise linear approximations. In temperature controllers, piecewise linear models are employed to control heaters based on temperature thresholds, resulting in distinct on-off behavior points in the response curve. Introducing polynomial nonlinearity in resonators by adding a term with coefficient β fundamentally alters the voltage-strain relationship within the piezoelectric equation, encapsulating the nonlinear disposition of the piezoelectric material under substantial strains. The primary system equations for m_m and m_r persistently portray the dynamics of the masses along with their reciprocal interactions, which remain unaffected by the inherent nonlinearity of the piezoelectric element. This incorporation of a nonlinearity parameter, β, facilitates a discernable softening behavior when it is positive and a hardening behavior when negative, each having distinct implications on resonance frequency and amplitude of vibration. Optimization of the nonlinear polynomial parameters can be a viable strategy for maximizing energy harvesting within the outlined system. This can be achieved by defining a cost function, an integration of power across a desired frequency span, thereby quantifying the performance. Utilizing computational tools, such as MATLAB, enables optimization of this function concerning the nonlinear coefficient. By examining the system's eigenvalues to extract information about the bandgap, a thorough combination of analytical and numerical methods is used to enhance the system's performance to achieve optimal results.

Figure 14 shows the relationship between the nonlinearity coefficient β and the harvested power in a monochain system. The $n = 8$ mass chain model is instrumental in depicting this correlation, serving as a concise yet representative framework to showcase the trends. Although a larger number of chains could enhance the metamaterial characteristic, the chosen size suffices to capture the essential dynamics for this analysis, aligning with the findings from Eq. (25).

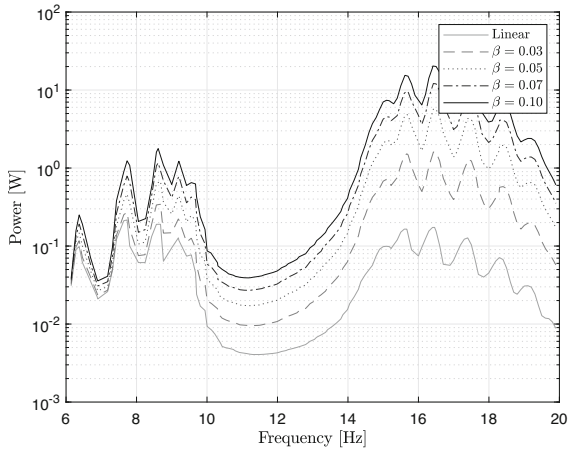

Fig. 14 Harvested power from a monochain with polynomial nonlinear local resonators in an eight-mass chain configuration. The graph highlights the impact of varying the nonlinearity coefficient β on the piezoelectric response and the resultant band gap behavior

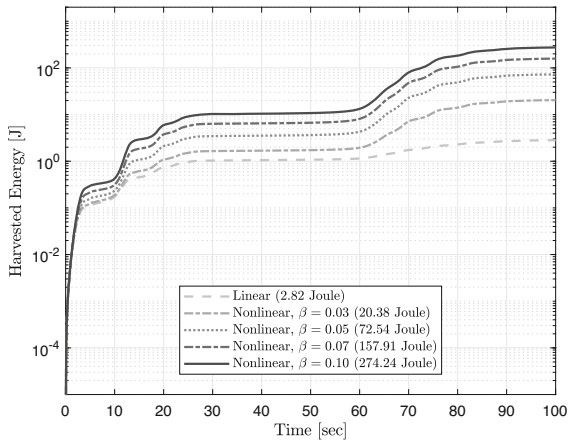

Fig. 15 Temporal Evolution of Harvested Energy: A depiction of energy harvested from piezoelectric elements over time in a monochain with polynomial nonlinear local resonators, utilizing $n = 8$ mass chains. This visualization underscores the profound influence of polynomial nonlinearity on the system's energy-harvesting trajectory, revealing a substantial enhancement in energy accumulation even in the absence of notable bandgap alterations

The interaction among β, vibration dynamics, and energy conversion can provide insights for enhancing energy collection in similar systems. Figure 15

delves into this concept, demonstrating how energy harvested from piezoelectric elements evolves over time. Although the introduction of polynomial nonlinearity doesn't significantly alter the formation of bandgaps, it noticeably impacts power and energy harvesting because of the increased motion in the presence of nonlinearity.

5.2 Model NL: 2-nonlinear capacitance in voltage-dependent scenarios

Starting with the general nonlinear equation in Eq. (27) and making a few simplifications, such as assuming consistent resistance, introducing voltage-dependent capacitance, transitioning from acceleration nonlinearity to velocity differences, and disregarding memory effects, the following model is derived to describe the nonlinear capacitance in the piezoelectric equation:

$$\frac{v(t)}{R} + c_p(v(t))\frac{dv(t)}{dt} - \theta\left(\frac{du_m(t)}{dt} - \frac{du_r(t)}{dt}\right) = 0 \tag{51}$$

Here, $c_p(v(t))$ represents the voltage-dependent capacitance, mathematically representing scenarios where capacitance shifts with applied voltage.

In practical applications, encountering nonlinear capacitance isn't rare and can be observed in various electronic components and systems like varactors, ferroelectric materials, and memristors. These systems showcase a capacitance that isn't static but modulates with the voltage applied, thereby exhibiting diverse behaviors across assorted operating regimes.

When simulating scenarios where capacitance nonlinearly shifts with voltage, an example relationship might be expressed as:

$$c_p(v(t)) = c_{p_0} + k_v \cdot v^2(t), \tag{52}$$

where k_v serves as a proportionality constant, illuminating and predicting how systems respond when capacitance dynamically interacts with applied voltage. In Fig. 16, a specific relationship between capacitance and voltage under the parameters $c_p = 1.5$ mF (base capacitance). The figure, composed of four subplots detailing Transmitance, Power, and Harvested Energy in relation to excitation frequency, and an illustration of the quadratic term coefficient of c_p piezo capacitance, provides a detailed overview of key data points. Notably, there's an evident increase in power when

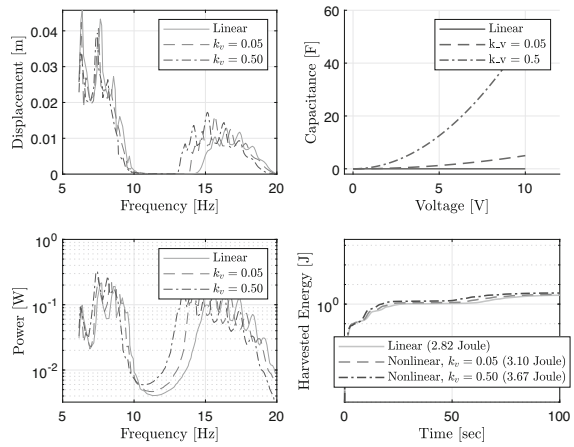

Fig. 16 Influence of quadratic nonlinear piezo capacitance, c_p on transmittance and harvested energy

dealing with nonlinear capacitance compared to linear piezo capacitance. This observation is corroborated by the energy acquired during the simulation time, which is 3.67 Joules, in contrast to the 2.82 Joules observed in a linear framework.

Thus, in this scenario, not only is more energy harvested from the resonators, but there is also an expansion in the transmittance bandgap. The dual advantages of vibration suppression in the main chain and enhanced energy harvesting from the resonator open the door to potentially more effective approaches for optimizing energy extraction in comparable systems.

5.3 Model NL: 3-cubic nonlinearities

Cubic nonlinearities can be found in electromechanical systems, such as sensors and actuators. In micro electromechanical systems (MEMS), such as accelerometers or gyroscopes, cubic nonlinearities can arise due to the miniaturized mechanical components. For nonlinear electromechanical coupling, the piezoelectric equation can be represented as:

$$\frac{v(t)}{R} + c_p\frac{dv(t)}{dt} - \theta\left(\frac{du_m(t)}{dt} - \frac{du_r(t)}{dt}\right)^3 = 0 \tag{53}$$

In Fig. 17, the relation between voltage $v(t)$ and relative displacement z is explored within the context of cubic nonlinearity. The subplot detailing the $v(t) - z(t)$ relationship illustrates that the equation simplifies to:

$$\frac{v(t)}{R} - \theta z(t)^n = 0 \tag{54}$$

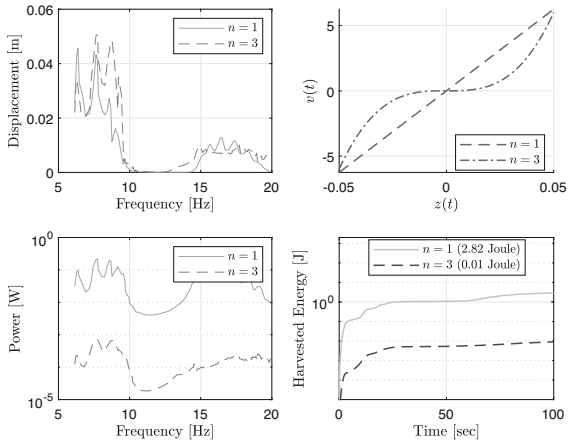

Fig. 17 Illustrating the Interplay of $v(t)$ and $z(t)$ in the Presence of Cubic Nonlinearities. The figure demonstrates how cubic nonlinearity affects electromechanical coupling in a piezoelectric system, utilizing specific resistances for standard and cubic terms (R = 500 Ω and R = 192 kΩ, respectively) to maintain consistent saturation characteristics across scenarios

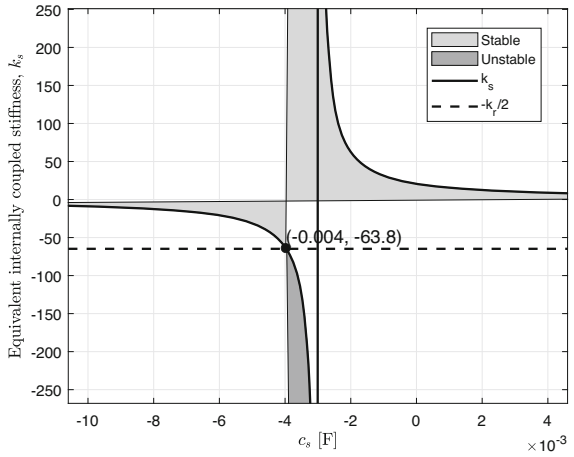

Fig. 18 Stability area of the electromechanical internally coupled lumped-mass system: Exploring the interplay between equivalent stiffness k_s and Shunt Capacitance c_s. Parameters: $n = 4$, $m_m = 56$ g, $m_r = 33.6$ g, $k_m = 150$ N/m, $k_r = 129.6$ N/m, $\theta = 0.25$ N/V, $R = 500\ \Omega$, $c_p = 1.5 \times 10^{-3}$ F

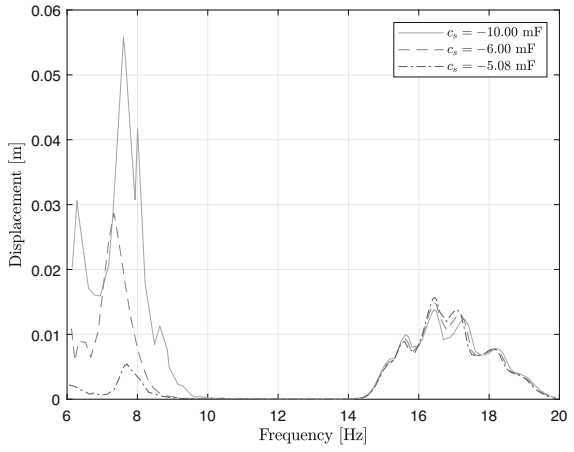

Fig. 19 Transmittance comparison of electrical internally coupling with shunt circuit for $\theta = 0.25$ and $c_p = 1.5$mF, demonstrating the impact of an equivalent negative stiffness

To maintain comparable saturation characteristics between a conventional linear resonator and one with a cubic term, resistances of $R = 500\Omega$ and 192 kΩ are utilized, respectively.

The case study demonstrates that introducing cubic nonlinear terms, linked to the relative velocities of the primary chain and resonator, significantly affects both harvested energy and transmittance. Specifically, the observed cubic nonlinearity contributes to a decline in harvested energy, posing noteworthy implications for optimization in energy-harvesting contexts, where strategies to circumvent or offset this reduction are crucial. Simultaneously, the incidence of these nonlinear terms provokes a contraction of the transmittance band gap, which could potentially affect the system's efficacy, inviting further exploration and mitigation strategy development.

6 Internally coupled resonators with electromechanical nonlinearity

Figure 18 visualizes the derived relationship of Eq. (48) and its implications for system stability. Based on the analysis, the threshold value of the equivalent internally coupled stiffness k_s for stability is given by $k_s > -\frac{k_r}{2}$. The relationship between k_s and shunt capacitance c_s is clearly illustrated, with the light gray region representing system stability and the dark gray region indicating system instability. The dividing threshold between these regions is represented by the line at $k_s = -\frac{k_r}{2}$. For the provided parameters, the system remains stable for c_s values ranging from negative infinity to approximately -0.004 Farad and resumes stability from around -0.003 Farad ($k_s = -3468$ to 5203 N/m) to positive infinity, with a brief interval of instability between these ranges. The magnified view offers a closer perspective on the critical transition points, emphasizing the pivotal c_s values at which the system's dynamical response alternates.

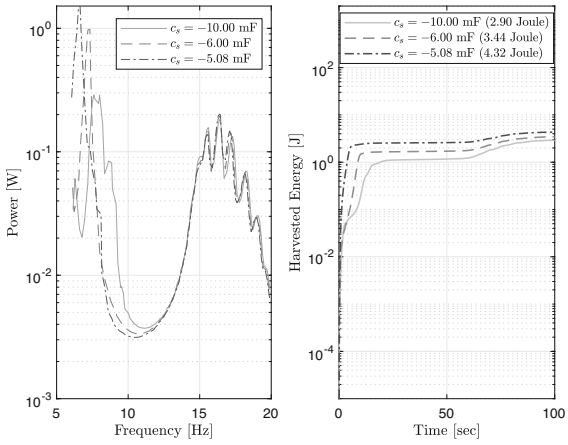

Fig. 20 Harvested power and energy across different shunt capacitances for $\theta = 0.25$ and $c_p = 1.5$mF

Figure 20 presents the harvested power and energy across a range of shunt capacitances. It clearly underscores the influential role of shunt capacitance on the system's overall efficiency. An observation made from the results is the superiority of electrical internal coupling via shunt circuits in terms of tunability. Specifically, electrical coupling seems to allow for easier tuning of the band gap compared to its mechanical counterpart. This is evident in Figs. 19 and 20, where the chosen shunt capacitor facilitates a band gap at a notably lower frequency in comparison to a mechanically internally coupled system, as illustrated in Fig. 9. Choosing a shunt capacitance of $c_s = -5.08$mF results in an equivalent stiffness of k_s = -30. This specific choice not only introduces an equivalent negative stiffness into the system, enhancing energy harvesting capabilities across varied frequency spectrums and enabling the creation of a lower-frequency band gap (see Fig. 19). Compared to mechanical internal coupling, this provides more flexibility in tuning the band gap across different frequencies.

7 Conclusion

This study utilized advanced mathematical modeling to analyze piezoelectric energy harvesters, delving into their mechanical and electrical dynamics. It elucidated the generalized formula for electromechanical nonlinearity and its impact on system performance. The insights gained from examining the interplay between nonlinear dynamics and energy harvesting efficiency have potential implications for optimizing such systems in future practical applications. The main contributions of this research include:

- The development and analysis of a comprehensive theoretical model for electromechanical nonlinearity, elucidating its significant impact on the performance of piezoelectric energy harvesters.
- A detailed examination of the band gap phenomenon in piezoelectric systems, revealing the significant impact of electromechanical parameters such as k_e and γ_3 on the energy harvesting process.
- An investigation into various models of nonlinearity within piezoelectric resonators, shedding light on the correlation between nonlinearity coefficients like β and the system's energy output.
- Insights into the benefits of employing nonlinear mechanical resonators within a mass chain, demonstrating an expansion of the band gap and an increase in energy harvesting potential.
- Observations on the effects of shunt capacitance and its role in internal resonator coupling, with implications for enhancing the energy harvesting capabilities of metamaterials.

The results underscore the intricate balance required between nonlinearity parameters and system efficiency, opening avenues for the optimization of energy harvesters in practical applications. Future studies are anticipated to delve deeper into electromechanical nonlinearity models, with an emphasis on scalability, parameter-specific impacts, and the development of feedback circuits for adaptive systems. The transition to distributed parameter models also stands out as a promising direction for achieving a closer representation of physical systems in piezoelectric energy harvesting research.

Funding This work has been supported by the European Union's Horizon Europe research and innovation program under the grant agreement No 101120657, project ENFIELD (European Lighthouse to Manifest Trustworthy and Green AI), by the Estonian Research Council through the grant PRG658, and by the Estonian Centre of Excellence in Energy Efficiency, ENER (grant TK230) funded by the Estonian Ministry of Education and Research.

Data availability The datasets supporting the conclusion of this article are included within the paper.

Declarations

Conflict of interest The authors declare that they have no conflict of interest.

References

1. Jiao, P., Mueller, J., Raney, J.R., Zheng, X., Alavi, A.H.: Mechanical metamaterials and beyond. Nat. Commun. **14**(1), 6004 (2023)
2. Liang, H., Hao, G., Olszewski, O.Z.: A review on vibration-based piezoelectric energy harvesting from the aspect of compliant mechanisms. Sens. Actuators A **331**, 112743 (2021)
3. Aldin, H.N., Ghods, M.R., Nayebipour, F., Torshiz, M.N.: A comprehensive review of energy harvesting and routing strategies for iot sensors sustainability and communication technology. Sens. Int., p. 100258 (2023)
4. Lee, G., Lee, D., Park, J., Jang, Y., Kim, M., Rho, J.: Piezoelectric energy harvesting using mechanical metamaterials and phononic crystals. Commun. Phys. **5**(1), 94 (2022)
5. Meninger, S., Mur-Miranda, J.O., Amirtharajah, R., Chandrakasan, A., Lang, J.: Vibration-to-electric energy conversion. In: Proceedings of the 1999 International Symposium on Low Power Electronics and Design, pp. 48–53 (1999)
6. Maurya, D., Yan, Y., Priya, S.: Piezoelectric Materials for Energy Harvesting. CRC Press, Boca Raton (2015)
7. Patil, G.U., Matlack, K.H.: Review of exploiting nonlinearity in phononic materials to enable nonlinear wave responses. Acta Mech. **233**(1), 1–46 (2022)
8. Daqaq, M.F., Masana, R., Erturk, A., Dane Quinn, D.: On the role of nonlinearities in vibratory energy harvesting: a critical review and discussion. Appl. Mech. Rev. **66**(4), 040801 (2014)
9. Daqaq, M.: Estimating the state-of-charge of a battery powered by a weakly nonlinear energy harvester (2024)
10. Li, Y., Baker, E., Reissman, T., Sun, C. and Liu, W.K.: Design of mechanical metamaterials for simultaneous vibration isolation and energy harvesting. *Appl. Phys. Lett.* **111**(25) (2017)
11. Tsujiura, Y., Suwa, E., Kurokawa, F., Hida, H., Kanno, I.: Reliability of vibration energy harvesters of metal-based pzt thin films. J. Phys.: Conf. Ser., vol. 557, p. 012096. IOP Publishing (2014)
12. Manktelow, K., Leamy, M.J., Ruzzene, M.: Multiple scales analysis of wave-wave interactions in a cubically nonlinear monoatomic chain. Nonlinear Dyn. **63**, 193–203 (2011)
13. Lepidi, M., Bacigalupo, A.: Wave propagation properties of one-dimensional acoustic metamaterials with nonlinear diatomic microstructure. Nonlinear Dyn. **98**(4), 2711–2735 (2019)
14. Zivieri, R., Garesci, F., Azzerboni, B., Chiappini, M., Finocchio, G.: Nonlinear dispersion relation in anharmonic periodic mass-spring and mass-in-mass systems. J. Sound Vib. **462**, 114929 (2019)
15. Bukhari, M., Joubaneh, E.F., Barry, O.: Spectro-spatial wave features in nonlinear metamaterials: theoretical and computational studies. J. Vib. Acoust. **143**(3), 031010 (2021)
16. Chaurha, A., Malaji, P.V., Mukhopadhyay, T.: Dual functionality of vibration attenuation and energy harvesting: effect of gradation on non-linear multi-resonator metastructures. Eur. Phys. J. Special Top. **231**(8), 1403–1413 (2022)
17. Xia, Y., Ruzzene, M., Erturk, A.: Dramatic bandwidth enhancement in nonlinear metastructures via bistable attachments. Appl. Phys. Lett., **114**(9) (2019)
18. Frazier, M.J., Kochmann, D.M.: Band gap transmission in periodic bistable mechanical systems. J. Sound Vib. **388**, 315–326 (2017)
19. Xia, Y., Ruzzene, M., Erturk, A.: Bistable attachments for wideband nonlinear vibration attenuation in a metamaterial beam. Nonlinear Dyn. **102**, 1285–1296 (2020)
20. Khasawneh, M.A., Daqaq, M.F.: Experimental assessment of the performance of a bi-stable point wave energy absorber under harmonic incident waves. Ocean Eng. **280**, 114494 (2023)
21. Lallart, M., Guyomar, D.: An optimized self-powered switching circuit for non-linear energy harvesting with low voltage output. Smart Mater. Struct. **17**(3), 035030 (2008)
22. Jiang, H., Wang, Y.: Research progress on piezoelectric energy harvesting circuits. Integr. Ferroelectr. **231**(1), 9–19 (2023)
23. Guyomar, D., Lallart, M.: Recent progress in piezoelectric conversion and energy harvesting using nonlinear electronic interfaces and issues in small scale implementation. Micromachines **2**(2), 274–294 (2011)
24. Yang, T., Zhou, S., Fang, S., Qin, W., Inman, D.J.: Nonlinear vibration energy harvesting and vibration suppression technologies: designs, analysis, and applications. Appl. Phys. Rev., **8**(3) (2021)
25. Silva, T.M.P., Clementino, M.A., de Sousa, V.C., De Marqui, C: An experimental study of a piezoelectric metastructure with adaptive resonant shunt circuits. IEEE/ASME Trans. Mechatron., **25**(2):1076–1083 (2020)
26. Norenberg, J.P., Cunha Jr, A., da Silva, S., Varoto, P.S.: Probabilistic maps on bistable vibration energy harvesters. Nonlinear Dyn., **111**(22), 20821–20840 (2023)
27. Chatterjee, T., Karlicic, D., Adhikari, S., Friswell, M.I.: Parametric amplification in a stochastic nonlinear piezoelectric energy harvester via machine learning. In: Data Science in Engineering, Volume 9: Proceedings of the 39th IMAC, A Conference and Exposition on Structural Dynamics 2021, pp. 283–291. Springer (2022)
28. Covaci, C., Gontean, A.: Piezoelectric energy harvesting solutions: a review. Sensors **20**(12), 3512 (2020)
29. Asanuma, H.: Electromechanical model and simple numerical analysis for a piezoelectric vibration energy harvester considering nonlinear piezoelectricity, nonlinear damping, and self-powered synchronized switch circuit. J. Intell. Mater. Syst. Struct. **34**(20), 2360–2378 (2023)
30. Lallart, M., Lombardi, G.: Synchronized switch harvesting on electromagnetic system: a nonlinear technique for hybrid energy harvesting based on active inductance. Energy Convers. Manage. **203**, 112135 (2020)
31. Tian, W., Zhao, Z., Liu, W., Zhu, Q., Zhang, Z., Yuan, Y.: Analysis on the power and bandwidth improvement of a frequency-tuning optimized sece circuit. Sens. Actuators A **332**, 113110 (2021)
32. Ahmad, F.F., Ghenai, C., Bettayeb, M.: Maximum power point tracking and photovoltaic energy harvesting for internet of things: a comprehensive review. Sustain. Energy Technol. Assess. **47**, 101430 (2021)
33. Li, D., Wang, C., Cui, X., Chen, D., Fei, C., Yang, Y.: Recent progress and development of interface integrated circuits for piezoelectric energy harvesting. Nano Energy **94**, 106938 (2022)

34. Boyan Stefanov Lazarov and Jakob Søndergaard Jensen: Low-frequency band gaps in chains with attached non-linear oscillators. Int. J. Non-Linear Mech. **42**(10), 1186–1193 (2007)
35. Zhou, W.J., Li, X.P., Wang, Y.S., Chen, W.Q., Huang, G.L.: Spectro-spatial analysis of wave packet propagation in nonlinear acoustic metamaterials. J. Sound Vib. **413**, 250–269 (2018)
36. Hu, G., Tang, L., Das, R.: Internally coupled metamaterial beam for simultaneous vibration suppression and low frequency energy harvesting. J. Appl. Phys., **123**(5) (2018)
37. Alimohammadi, H., Vassiljeva, K., HosseinNia, S.H., Petlenkov, E.: Exploring internally coupled resonator's dynamics and spatial variability in metamaterials for vibration suppression. In: Active and Passive Smart Structures and Integrated Systems XVIII (2024)
38. Shu, Y.C., Lien, I.C.: Analysis of power output for piezoelectric energy harvesting systems. Smart Mater. Struct. **15**(6), 1499 (2006)
39. Alimohammadi, H., Vassiljeva, K., HosseinNia, S.H., Petlenkov, E.: Stability analysis and energy harvesting in lumped parameter systems with internally coupled resonators. J. Vib. Control (2024)
40. Manimala, J.M., Sun, C.T.: Numerical investigation of amplitude-dependent dynamic response in acoustic metamaterials with nonlinear oscillators. J. Acoust. Soc. Am. **139**(6), 3365–3372 (2016)